Chemical Papers (2022) 76:2747–2758
https://doi.org/10.1007/s11696-021-02059-y

ORIGINAL PAPER

Theoretical investigation on the intermolecular interactions between 3-nitro-1,2,4-triazol-5-one and 2,6-diamino-3,5-dinitropyrazine-1-oxide using DFT methods

Wen-jun Hu[1,2] · Rui-jun Gou[1] · Shu-hai Zhang[1] · Yang Liu[1] · Feng-qin Shang[3] · Ya-hong Chen[1] · Hui Bai[1]

Received: 13 October 2021 / Accepted: 29 December 2021 / Published online: 13 January 2022

Abstract
The intermolecular interactions between the insensitive explosives 3-nitro-1,2,4-triazol-5-one (NTO) and 2,6-diamino-3,5-dinitropyrazine-1-oxide (LLM-105) in the TNT-based melt cast explosive were theoretically investigated with the density functional theory method (DFT). The structures of NTO/LLM-105 complexes were optimized. Five stable structures were optimized using molten 2,4,6-trinitrotoluene (TNT) as an implicit solvent for correction. The types and distribution of intermolecular interactions were analyzed using reduced density gradient (RDG) analysis, and the hydrogen bond strengths were studied by core-valence bifurcation (CVB). The results are shown that the intermolecular interactions between NTO and LLM-105 were dominated by N–H…O type hydrogen bonds, and the strongest hydrogen bonds were between the hydrogen atom (H6) in the molecular of NTO and the oxygen atom (O13) in the molecule of LLM-105. The intermolecular hydrogen bond strength is ranked as Structure I > Structure II > Structure IV > Structure III > Structure V, which determines the stability of the structure. It is obvious that Structure I is the stablest. The results contribute to the investigation of the performance for melt cast explosives as well as provide guidance for explosive formulation design.

Keywords Intermolecular interactions · NTO · LLM-105 · Hydrogen bonding

Introduction

The key driving force in modern energetic materials research is the development of high energy, low sensitivity materials for future applications in insensitive munitions (IMs). Melt cast explosives have played a significant role in IMs due to the simplicity of forming the charges (Ravi et al. 2011). Conventional melt cast explosives are formed by casting 2,4,6-trinitrotoluene (TNT) or its mixtures with 1,3,5-trinitro-1,3,5-triazine (RDX) or 1,3,5,7-tetranitro-1,3,5,7-tetrazocine (HMX) (Badgujar and Talawar 2018; Li et al. 2019). With the increasing demand for melt cast explosives, the replacement for RDX and HMX in TNT melt cast explosive has attracted much attention from both experimentalists and theoreticians (Badgujar and Talawar 2017, 2018; Mishra et al. 2017; Sarangapani et al. 2015).

3-Nitro-1,2,4-triazol-5-one (NTO) is a high energy, insensitive energetic material with a crystal density of 1.93 g/cm^3. Its theoretical explosive velocity is 8670 m/s, which is comparable to RDX (Lee et al. 1987; Smith and Cliff 1999; Powala et al. 2006; Hang et al. 2018). However, the impact sensitivities of NTO are significantly superior to those of HMX and RDX (Liu et al. 2019). Therefore, NTO may serve as a series of promising alternatives to RDX and HMX (Vijayalakshmi et al. 2015). A series of NTO-based melt cast explosives had been reported (Trzcinski et al. 2016; Trzcinski 2020). Though it has high detonation performance and excellent safety, NTO exhibits a high level of acidity (pKa = 3.76) which has substantially limited its application (Wu et al. 2015). NTO also has a high viscosity during processing due to its needle-like crystal structure. 2,6-Diamino-3,5-dinitropyrazine-l-oxide (LLM-105) is studied as a highly promising alternative due to its remarkable thermal stability and insensitivity to spark, friction, and shock (Li et al.

✉ Rui-jun Gou
grjzsh@163.com

[1] College of Environmental and Safety Engineering, North University of China, Taiyuan 030051, Shanxi, People's Republic of China

[2] National Key Laboratory of Applied Physics and Chemistry, Xi'an 710061, Shaanxi, People's Republic of China

[3] Research Institute of Gansu Yin'guang Chemical Industry Group, Baiyin 730900, People's Republic of China

2016; Wang et al. 2018; Jun et al. 2021). The sensitivities and performance parameters of RDX, HMX, NTO and LLM-105 are presented in Table 1 (Klapötke 2021; Badgujar et al. 2008; Peterson et al. 2007). The advantage of LLM-105 compared to other insensitive explosives is its superior thermal stability. The thermal decomposition temperature is 354 °C. It is 150 °C higher than RDX's. Moreover, it is compatibility with TNT, 2,4,6,8,10,12-Hexanitrohexaazaisowurtzitane (CL-20), 1,1-Diamino-2,2-Dinitroethene (FOX-7), HMX et al. (Li et al. 2017; Zhang et al. 2020). Therefore, it is suitable to add into melt cast explosives. In addition, in the structure of LLM-105, the triazole ring shows good planarity, bonding an extra oxygen atom (Mason et al. 2019). This particular structure provides the opportunities to form hydrogen bonds with NTO, which decreases the acidity of the NTO. Therefore, NTO/LLM-105 complexes are wished to improve the performance of NTO-based melt cast explosives.

During the last few decades, with the development of quantum chemistry (Firme 2021), density functional theory with dispersion correction (DFT-D3) is often used to study intermolecular interactions (Alipour and Taravat 2018; Grimme et al. 2010; Grimme 2011). The degradation mechanism of NTO in water was studied in the 6-311 + (g, d) basis using the M06-2X functional. The results suggest that hydroxide ions accelerate the degradation of NTO in water (Wang and Shukla 2021). The crystal structure, electronic properties, intermolecular interactions and dynamic properties of β-NTO crystals were investigated using density functional tight binding (DFTB) and DFTB-based molecular dynamics (DFTB-MD). The introduction of impurities enhances O···H and O···O interactions but decrease N···O interactions (Ji et al. 2021). NTO dimers were studied at the DFT-B3LYP level by the Berny method with 6-311++G** basis set. Atomic charges and natural bond orbital analyses on the dimers were also performed to probe the origin of the interactions (Xiao et al. 2004). Researchers investigate the type, strength and distribution of intermolecular interactions by calculating binding energies, non-covalent interaction maps, electron cloud density and other analytical methods (Zhu et al. 2017; Duarte et al. 2019; Li et al. 2021; Kaur and Khanna 2011; Pina et al. 2021; Hammami et al. 2021; Gopalakrishnan et al. 2018). However, investigations of the interaction mechanism between NTO molecules and LLM-105 molecules are rare. Therefore, in this work, the DFT-D3 was used to investigate the interaction between NTO molecules and LLM-105 molecules in molten TNT, in order to provide the helpful for the design and production of higher performance melt cast explosives.

Table 1 Performance parameters

	NTO	LLM-105	RDX	HMX
ΔH_f [a] (kJ/mol)	−96.7	−12.97	86.3	75
ρ [b] (g/cm^3)	1.93	1.913	1.816	1.91
O.B.[c] (%)	−24.60	−37.02	−21.61	−21.61
D [d] (GPa)	31.2	35	33.92	38.39
VOD[e] (m/s)	8670	8560	8600	9100
T_{dec} [f] (°C)	258	354	208	276
$H_{50\%}$ [g] (cm)	93	117	71	65
F.S.[h] (kg)	> 36	> 36	12	13.8

[a]Heat of formation
[b]Density
[c]Oxygen balance
[d]Detonation pressure
[e]Detonation velocity
[f]The thermal decomposition temperature
[g]Impact sensitivity
[h]Friction sensitivity

Simulation method

All calculations were carried out with the Gaussian 09 package (Frisch et al. 2009). The initial structures of NTO and LLM-105 were extracted from the Cambridge Crystallographic Data Center (CCDC) database (Bolotina et al. 2003; Averkiev et al. 2002). Molecular structures of NTO and LLM-105 monomer had been optimized at the B3LYP-D3 levels with the 6-311++G(d, p) basis sets using the molten TNT as an implicit solvent for correction. Then, the Genmer package (Lu Version1.9.9) was used to generate 50 structures of NTO/LLM-105 complex. In addition, the Molclus package was used to invoke the quantum chemistry program. Minimum energy structures were selected by geometric optimization and energy calculation, respectively, and minima were verified as having no imaginary vibrational frequencies. The five minimum energy structures of NTO and LLM-105 were selected as the subjects for analysis by using molten TNT as the implicit solvent for correction. Interaction energy was analyzed based on these structures. In addition to, atoms in molecules (AIM) topological analysis of electron density at the bond critical point, reduced density gradient (RDG) analysis, nitro group charge analysis, electrostatic potential analysis and hydrogen bond core-valence bifurcation (CVB) index analysis were studied by the Mutiwfn package (Lu and Chen 2012). These analytical methods were used to study the type, location and strength of weak intermolecular interactions.

The intermolecular interaction energy E(int.) is calculated by the basis set superposition error (BSSE), which uses the counterpoise correction (CP) to correct. The interaction energy of the system is calculated by Eq. (1).

$$E(\text{int}) = E(\text{NTO/LLM} - 105) - E(\text{NTO}) - E(\text{LLM} - 105) + E(\text{BSSE}) \quad (1)$$

where E(NTO/LLM-105) is the total energy of the complexes, E(NTO) is the energy of single molecule of NTO, E(LLM-105) is the energy of single molecule of LLM-105, and E(BSSE) is the CP correction energy.

Restrained electrostatic potential (RESP) charge, which is arguably the most suitable atomic charge of flexible small molecules for molecular simulations. It uses the analysis of the difference in electron density and the amount of change in nitro group charge to explain the effect of intermolecular interactions. The nitro group charge Eq. (2) is

$$Q(NO_2) = Q(N) + Q(O1) - Q(O2) \quad (2)$$

where $Q(NO_2)$ is the nitro group charge; Q(N) is the nitrogen atom charge; and Q(O1) and Q(O2) are each two oxygen atom charges on the nitro group.

Results and discussion

Structures

The stable structures of NTO and LLM-105 monomer were optimized at the B3LYP-D3/6-311++G (d, p) basis sets as shown in Fig. 1. The major bond lengths are compared with the experimental data. It is found that the error between calculated and experimental values is 3.6% for the NTO molecule, 0.67% for the LLM-105 molecule (Table 2), which are basically consistent with the experimental data and verify the feasibility of the calculated structures.

The stable structures of the five minimum energy NTO and LLM-105 complexes were optimized with the implicit solvent TNT, as shown in Fig. 2. We can find that the intermolecular interaction between NTO and LLM-105 exists mainly between hydrogen and oxygen atoms, and the distance between H…O ranges from 1.6826 to 2.0163 Å, as shown in Table 3. The sum of the radii of the hydrogen and oxygen atoms is 2.75 Å, and it falls within the range of atomic distances for hydrogen bonding interactions. Therefore, it is concluded that there are probably hydrogen bonds between molecules. From Fig. 3, it can be shown that among the five structures, the H(6) in the NTO molecular is tend to form a hydrogen bond with the oxygen atom in the LLM-105 molecule. But the hydrogen bond cannot be observed in Structure IV. This means that H(6) in NTO is more active, which facilitates the formation of hydrogen bonds between NTO and LLM-105 to decrease the acidity of the NTO.

It was found that the hydrogen bonds in the structure I and II are formed between H(6) in the NTO molecule and O(13) in the LLM-105 molecule. The hydrogen bonds in Structure III and V are formed between H(6) and the oxygen atom on the nitro group in the LLM-105. The hydrogen bonding distance of H6…O13 is significantly shorter than the hydrogen bonding distance of H(6)…O(17) and H(6)…O(24), indicating H(6)…O(13) interaction is more powerful than H(6)…O(17) and H(6)…O(24). It is also shown that the hydrogen bonding interaction of Structure I and Structure II is more powerful than that of Structure III and Structure V.

In order to compare with the dimer of NTO and the dimer of LLM-105, the five minimum energy structures of

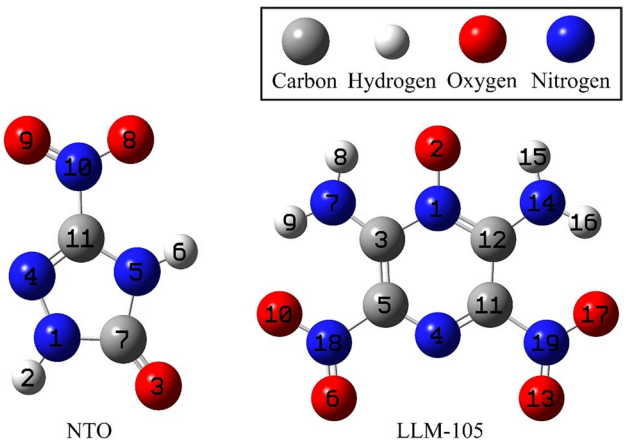

Fig. 1 Molecular structure graph of NTO and LLM-105

Table 2 Main bond length for molecules NTO and LLM-105

NTO	Exp	Cal	LLM-105	Exp	Cal
N(1)–H(2)	0.862	1.0082 (16.9)	N(1)–O(2)	1.308	1.3002 (0.60)
N(5)–H(6)	0.904	1.0086 (11.6)	C(3)–N(7)	1.320	1.3274 (0.56)
C(3)–O(7)	1.235	1.2043 (−2.5)	C(12)–N(14)	1.308	1.3274 (1.48)
C(11)–O(10)	1.444	1.4496 (0.4)	C(5)–N(18)	1.458	1.4720 (0.96)
N(10)–O(8)	1.231	1.2302 (−0.1)	N(18)–O(6)	1.216	1.2104 (0.46)
N(10)–O(9)	1.222	1.2149 (−0.6)	N(18)–O(10)	1.237	1.2393 (0.18)
N(1)–N(4)	1.370	1.3584 (−0.8)	C(5)–O(4)	1.314	1.3071 (0.52)
			C(11)–O(4)	1.315	1.3071 (0.60)
Average deviation /%		3.6	Average deviation /%		0.67

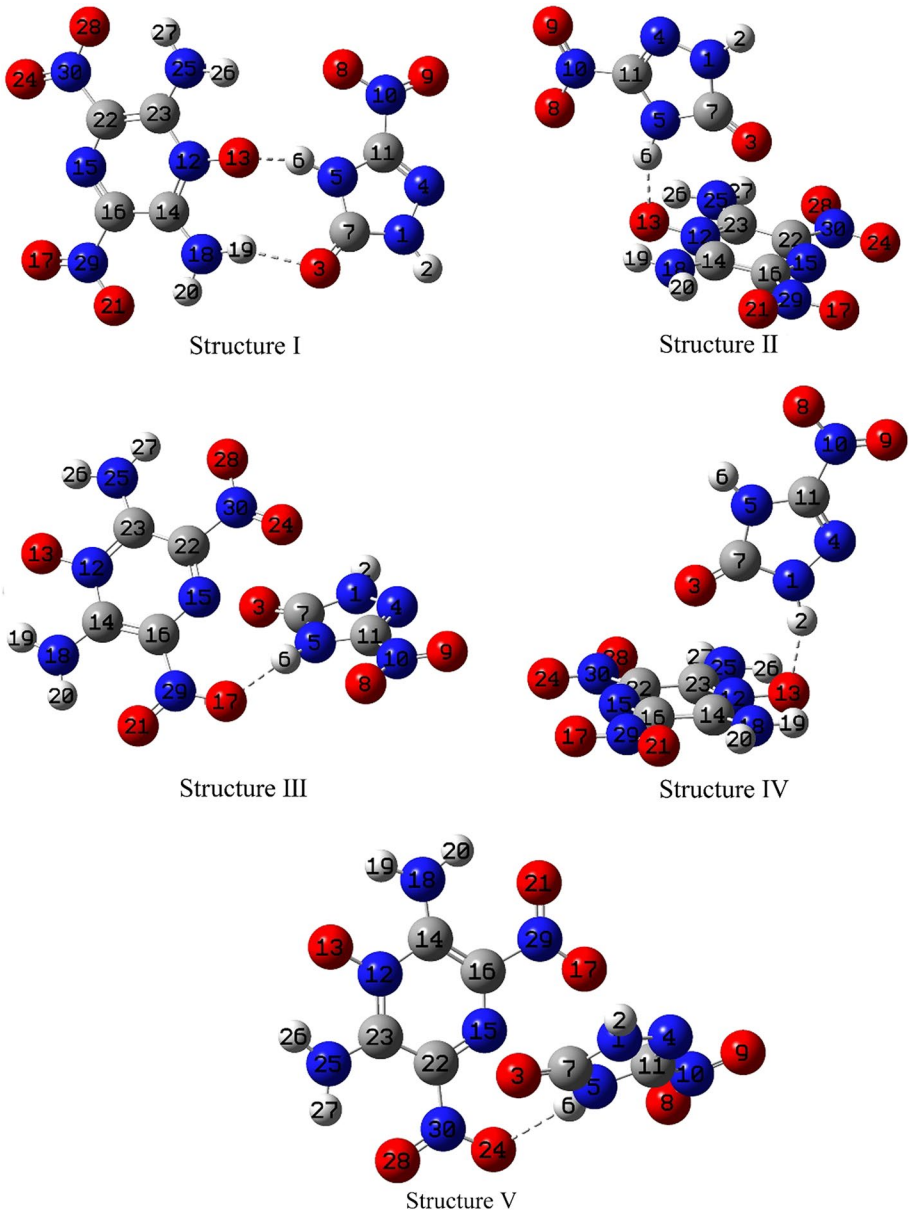

Fig. 2 Five structures of NTO and LLM-105 complex; calculated at B3LYP-D3/6-311++G (d, p) basis sets

Table 3 Hydrogen bonds length

NTO/LLM-105			NTO dimer		
Structure	Interaction	Length (Å)	Structure	Interaction	Length (Å)
I	H(6)…O(13)	1.6826	VI	H(13)…O(3)	1.7884
	H(3)…O(19)	1.9715		H(6)…O(14)	1.7648
II	H(6)…O(13)	1.7577	VII	H(2)…O(14)	1.7960
III	H(6)…O(17)	1.9351		H(13)…O(3)	1.7960
IV	H(2)…O(13)	1.8061	VIII	H(13)…O(3)	1.8649
V	H(6)…O(24)	2.0163	IX	H(2)…O(19)	1.9655
				H(17)…O(3)	1.7676
			X	H(6)…O(14)	1.7664
				H(17)…O(8)	1.9601

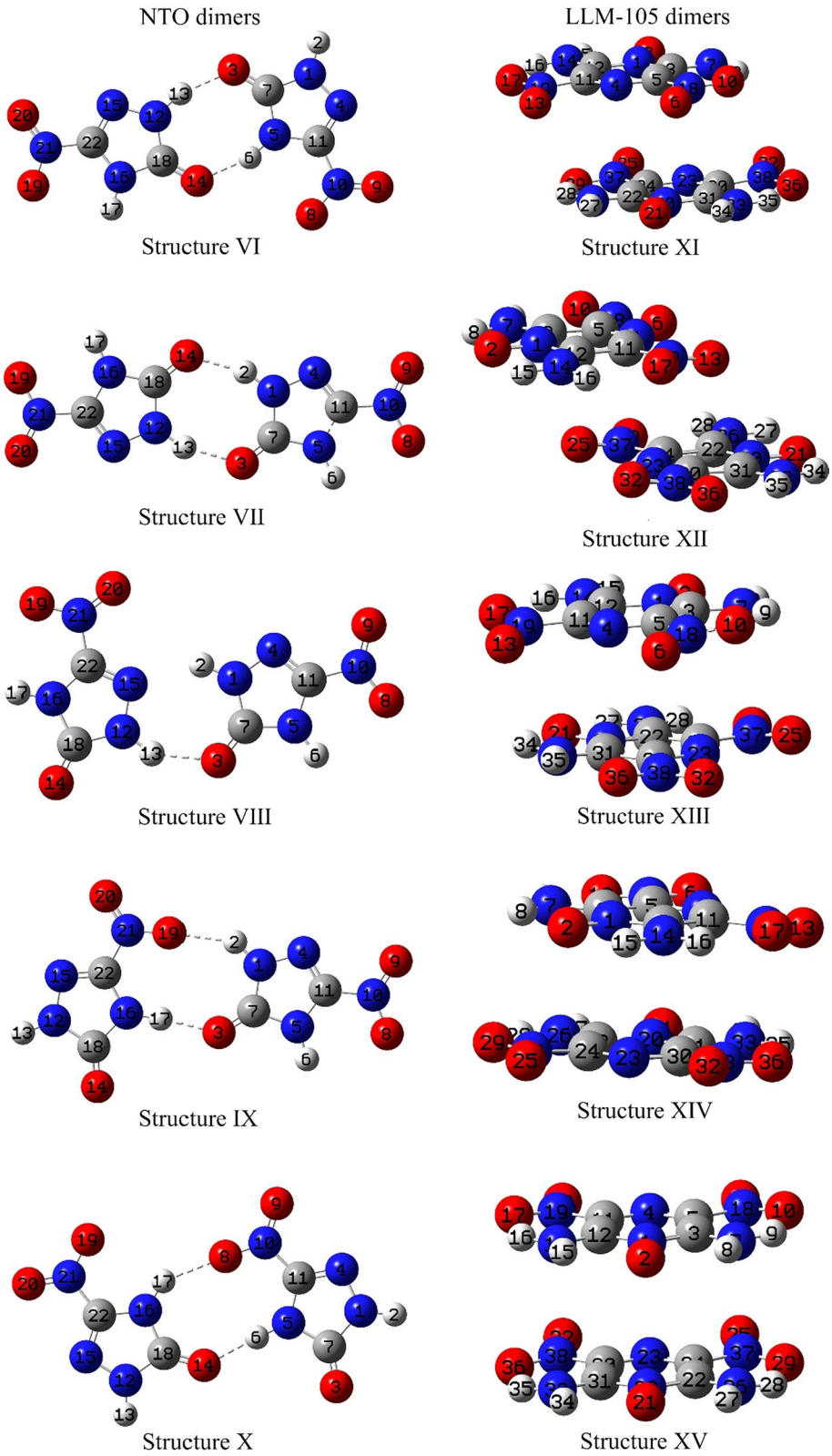

Fig. 3 Structures of NTO dimer and LLM-105 dimer at B3LYP-D3/6-311++G (d, p) basis sets

NTO (Structure VI, Structure VII, Structure VIII, Structure IX, Structure X) and the five minimum energy structures of LLM-105 (Structure XI, Structure XII, Structure XIII, Structure XIV, Structure XV) were optimized at B3LYP-D3/6-311++G (d, p) basis sets by the same method (Fig. 3). Hydrogen bonds are formed between NTO dimer molecules (Table 3). The LLM-105 dimer is arranged in a laminar pattern with π-stacking interactions, and hydrogen bonding cannot be observed. It is obvious that the H(6)…O(13) hydrogen bond lengths in Structure I are shorter than any hydrogen bond lengths between the NTO dimer molecules. Therefore, the interaction between NTO and LLM-105 molecules is stronger than NTO dimer also stronger than LLM-105 dimer.

Interaction energy analysis

To further investigate the stability of the structures, with the implicit solvent TNT, the intermolecular interaction energy E(int.) was calculated at the B3LYP-D3/6-311++G (d, p) basis set level (Table 4). The intermolecular interaction energies of NTO /LLM-105 complex were ordered as: Structure I (− 69.41 kJ/mol) < Structure II (− 57.95 kJ/mol) < Structure IV (− 55.56 kJ/mol) < Structure III (− 54.64 kJ/mol) < Structure V (− 53.64 kJ/mol). Generally, the interaction energy of hydrogen bond is in the range of − 160 ~ − 16 kJ/mol (Steiner 2010). The lower the energy, the more stable the structure is. Therefore, the hydrogen bonds dominate the intermolecular interactions in the NTO/LLM-105 complex. By comparing the intermolecular interaction energy of the NTO/ LLM-105 complex with the NTO dimer and the LLM-105 dimer, it was found that Structure I has the smallest interaction energy and thus the most stable structures. It indicates the existence of a more stable structure of NTO/LLM-105 complex than that of the dimers.

The interaction energies of NTO/LLM-105 complex were also calculated at M062X-D3/6-311++G (d, p) basis set level. The two different levels of interaction energy are shown in Fig. 4. It can be shown that the interaction energies were calculated at M062X-D3/6-311++G (d, p) levels are slightly higher than those were calculated at the B3LYP-D3/6-311++G (d, p) level. However, the same trend was observed at both levels. Therefore, the stability ranking

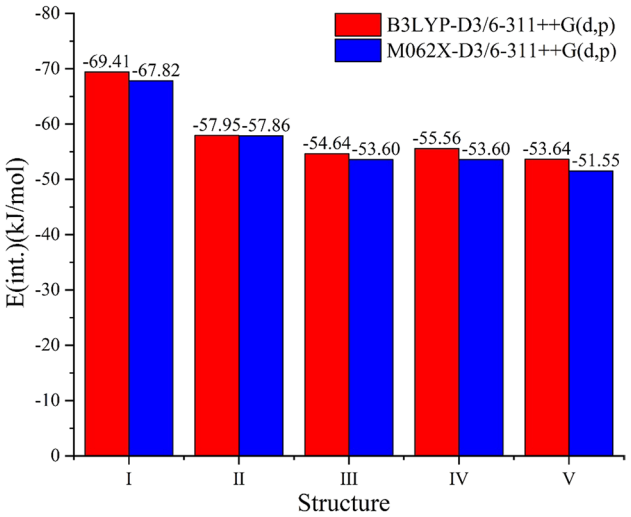

Fig. 4 Interaction energy of NTO/LLM-105 complexes at the B3LYP-D3/6-311++G (d, p) basis sets and the M062X-D3/6-311++G(d, p) basis sets

of the 5 structures is: Structure I > Structure II > Structure IV > Structure III > Structure V. It is obvious that Structure I is the stablest.

Electron density topology analysis

The AIM electron density topology analysis at the bond critical point can effectively study the intermolecular interactions and analyze the essence of the interactions (Bader and Stephens 1975; Lu and Chen 2013). The total electron density $\rho(r)$ at 0.002 ~ 0.04 a.u., which shows the hydrogen bonding. The closer its value is to 0.04, the better interaction performance it demonstrates (Waller and Yang 2013). Laplacian of the electron density $\nabla^2\rho(r)$ and the energy density $H(r)$ represents the type of intermolecular interactions. The $H(r)$ is calculated by Eq. (3).

$$H(r) = V(r) + G(r) \tag{3}$$

where the $V(r)$ is the potential energy density, and $G(r)$ is Lagrangian kinetic energy.

Table 4 Interaction energies E(int.)

Structure	NTO/LLM-105 complex	NTO dimer	LLM-105 dimer
E(int.) (kJ/mol)	− 69.41 (I)	− 65.60 (VI)	− 65.56 (XI)
	− 57.95 (II)	− 63.84 (VII)	− 65.56 (XII)
	− 54.64 (III)	− 57.36 (VIII)	− 54.18 (XIII)
	− 55.56 (IV)	− 56.94 (IX)	− 47.53 (XIV)
	− 53.64 (V)	− 56.27 (X)	− 46.74 (XV)

The negative value of the $\nabla^2\rho(r)$ represents covalent bonding interactions, and the positive value of the $\nabla^2\rho(r)$ represents hydrogen bonding and van der Waals interactions (Cremer and Kraka 1984). From Table 5, $\rho(r)$ of the NTO/LLM-105 complexes ranged from 0.00191 to 0.0437 a.u. Values of $\nabla^2\rho(r)$ are positive. Therefore, NTO/LLM-105 complexes exhibit stable hydrogen bonding and van der Waals interactions. The maximum $\rho(r)$ values for the five complexes in the NTO/LLM-105 structures are 0.0457 a.u. (Structure I H(6)…O(13)) > 0.0390 a.u. (Structure II H(6)…O(13)) > 0.0364 a.u. (Structure IV H(2)…O(13)) > 0.0236 a.u. (Structure I H(3)…O(19)) = 0.0236 a.u. (Structure III H(6)…O(17)) > 0.0202 a.u. (Structure V H(6)…O(24)). It is shown that the dominating intermolecular interactions between NTO and LLM-105 are H(6)…O(13) and H(2)…O(13). The stronger hydrogen bonds were observed in Structure I, II and IV (Table 6).

Reduced density gradient analysis

Weak interacting regions can be visualized using reduced density gradient (RDG) analysis. This method is an extension of the atoms in molecules (AIM) method. In order to distinguish numerically between regions of the system with different characteristics, a time–space function (4) is defined.

$$\mathrm{RDG}(r) = \frac{1}{2 \times \left(3 \times \pi^2\right)^{1/3}} \times \frac{\left|\nabla^2 \rho(r)\right|}{\rho(r)^{4/3}} \tag{4}$$

Combining the RDG(r) function and the $\rho(r)$ function determines those regions in the molecule that are implicated in weak interactions. The RDG closed equivalence surface generally encloses the corresponding critical point, and the larger the value of $\rho(r)$, the stronger the interaction. Each point in the scatter plot represents a single grid, and the density of the points indicates a higher electron density and

Table 5 Topological parameters of electron density at the bond critical point for NTO/LLM-105 complex (a.u.)

Structure	Interaction	$\rho(r)^a$	$\nabla^2\rho(r)^b$	$V(r)^c$	$G(r)^d$	$H(r)^e$
I	H(6)…O(13)	0.0457	0.1434	−0.0438	0.0398	−0.0040
	H(3)…O(19)	0.0236	0.0844	−0.0168	0.0189	0.0022
II	H(6)…O(13)	0.0390	0.01189	−0.0334	0.0316	−0.0019
III	H(6)…O(17)	0.0236	0.0902	−0.0174	0.0199	0.0026
IV	H(2)…O(13)	0.0364	0.1141	−0.0303	0.0294	−0.0009
V	H(6)…O(24)	0.0202	0.0779	−0.0142	0.0168	0.0027

[a]The density of all electrons

[b]Laplacian of the electron density

[c]The potential energy density

[d]Lagrangian kinetic energy

[e]The energy density

Table 6 Nitro group charge of NTO/LLM-105 complexes

Structure	Molecule	Parameter	Charge/e		
			Monomer	Complex	Δ(M-C)
I	NTO	O(8)–N(10)–O(9)	−0.10727	−0.11714	0.0099
	LLM-105	O(17)–N(29)–O(21)	−0.11666	−0.12323	0.0066
		O(24)–N(30)–O(28)	−0.11786	−0.12451	0.0066
II	NTO	O(8)–N(10)–O(9)	−0.10727	−0.11522	0.0079
	LLM-105	O(17)–N(29)–O(21)	−0.11666	−0.11254	−0.0041
		O(24)–N(30)–O(28)	−0.11786	−0.11254	−0.0053
III	NTO	O(8)–N(10)–O(9)	−0.10727	−0.11345	0.0062
	LLM-105	O(17)–N(29)–O(21)	−0.11666	−0.07973	−0.0369
		O(24)–N(30)–O(28)	−0.11786	−0.10181	−0.0160
IV	NTO	O(8)–N(10)–O(9)	−0.10727	−0.13602	0.0287
	LLM-105	O(17)–N(29)–O(21)	−0.11666	−0.11167	−0.0050
		O(24)–N(30)–O(28)	−0.11786	−0.11165	−0.0062
V	NTO	O(8)–N(10)–O(9)	−0.10727	−0.09131	−0.0160
	LLM-105	O(17)–N(29)–O(21)	−0.11666	−0.10312	−0.0135
		O(24)–N(30)–O(28)	−0.11786	−0.07045	−0.0474

stronger interactions. In Fig. 5, the position of hydrogen bonds can be observed, and the colors represent the type of interaction. The blue region ($\text{sign}(\lambda_2) < 0$) represents the stronger interactions (hydrogen bonds). The green region represents a weaker interaction (van der Waals). The red region ($\text{sign}(\lambda_2) > 0$) represents the repulsive interactions.

As can be observed in the scatter plot (Fig. 5), when $\text{sign}(\lambda_2) < -0.01$ a.u., a clear blue wave peak appears. It indicates that hydrogen bonding exists in five structures of NTO/LLM-105 complex, and the denser the point the stronger the hydrogen bonding effect. In contrast, the $\text{sign}(\lambda_2)$ ρ value in Structure I is at $-0.01.\sim 0$ a.u., and there is no obvious wave; therefore, van der Waals interaction is small. The intermolecular interactions in Structure I are mainly hydrogen bonds. In other structures, $\text{sign}(\lambda_2)$ ρ values at $-0.01.\sim 0$ a.u., green wave peaks appear, indicating that NTO/LLM-105 complexes exhibit hydrogen bonding and van der Waals interactions. The conclusions drawn are consistent with the AIM electron density topology analysis.

Nitro group charge analysis

Atomic charge is the most common model to describe the charge distribution of the interaction. The more negative the nitro group charge of the energetic material, the lower its impact sensitivity. It has been shown that there is a relationship between the H_{50} and the charge of the nitro group: When the nitro group has a charge of less than -0.23e, the H_{50} is less than 0.4 m (Zhang et al. 2005). The restrained electrostatic potential (RESP) is used to describe the nitro group charge in the NTO/LLM-105 complexes.

It was found that compared with the single-molecule nitro group charges, the nitro group charges of NTO in Structure I, II, III and IV decreased by 0.0099e, 0.0079e, 0.0062e and 0.0287e, respectively. All the nitro group charges in Structure I decreased; therefore, it has the lowest sensitivity. The analysis was shown that when intermolecular interactions were formed between NTO and LLM-105. There is a general decrease in the charge of nitro group within the NTO molecule. Therefore, the sensitivity of NTO is decreased.

Analysis of molecular surface electrostatic potential

The electrostatic potential is important for interactions due to its crucial influence on predicting reaction sites and predicting molecular properties. By drawing the diagram, the electrostatic potential of each monomer is colored into a molecular surface map. From it, the location of interpenetration on the van der Waals surface can be clearly seen. The strength of the interactions can be observed. The positive phase is shown in red, while the negative one is shown in blue. Figure 6 shows the electrostatic potential on the surface of single molecules of NTO and LLM-105. From the figure, it can be found that the NTO single-molecule electrostatic potential diagram has electrostatic potential maxima on the surface of hydrogen.

However, the nitro group and carbonyl groups in the geometry of NTO molecule have a strong electrostatic attraction effect, and there is an electrostatic potential minimum (-123.34 kJ/mol) on the surface of the molecule located near the oxygen on the nitro group. Since both electron-attraction groups are in the neighboring position of N(5) and have a strong electron-attraction effect on it at the same time, the density of electron cloud on the N(5) is decreased. The H(6) is more easily ionized. The value of the electrostatic potential on the molecular surface near the hydrogen atom is higher, which verifies the reason for the acidic nature of the NTO.

The electrostatic potential on the surface of the LLM-105 molecule shows that the point of minimal value of the electrostatic potential is near the N(13) atom (-147.28 kJ/mol). It is easier to form an electrostatic attraction with the hydrogen atoms on the NTO molecule.

The region of hydrogen bond can be observed from Fig. 7. The red and blue colors penetrate each other, reflecting the complementary characteristics of the electrostatic potential. This indicates that there is a strong attraction between NTO and LLM-105 molecules, which is conducive to the formation of stable complexes. The hydrogen bonding interactions formed by H(6)…O(13) in Structure I, II and IV, with the red and blue electrostatic potentials penetrating each other. It is shown that the hydrogen bond between NTO and LLM-105 is easily formed.

Hydrogen bond core-valence bifurcation (CVB) index analysis

The CVB index is another important value which can evaluate the strength of hydrogen bonds. The CVB index of relatively strong hydrogen bonds is generally significantly negative; very strong hydrogen bonds with distinct covalent characteristics can reach very negative values; the CVB index of strong hydrogen bonds is generally around 0; and the CVB index of weaker hydrogen bonds is generally positive. The CVB indices of hydrogen bonds in the five structures of NTO/LLM-105 complexes are shown in Fig. 8. It can be clearly observed that the CVB index values are in order of magnitude: Structure I < Structure II < Structure IV < Structure III < Structure V. Then, the strength of the intermolecular hydrogen bond is ranked as Structure I > Structure II > Structure IV > Structure III > Structure V. The positive CVB of Structure III and Structure V shows that the interaction is weak hydrogen bonding in these two structures, and the negative CVB indices of the remaining structures indicate stronger hydrogen bonding. The strong hydrogen bonding interaction can be formed between NTO

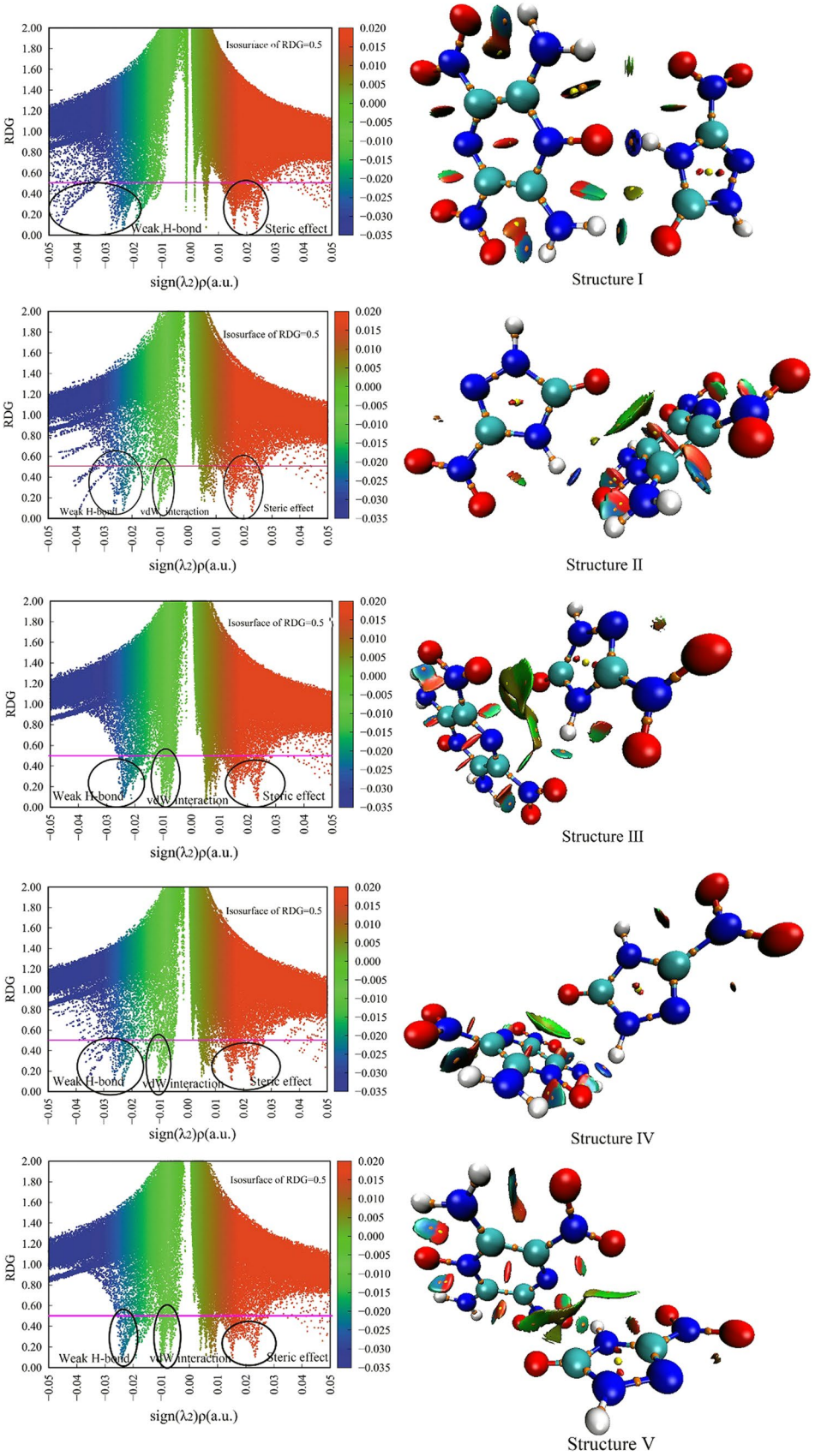

Fig. 5 The scatter diagram, isosurface graph of RDG and AIM for structures of NTO/LLM-105 complex

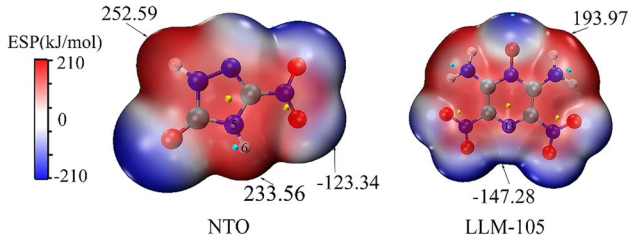

Fig. 6 NTO and LLM-105 single-molecule surface electrostatic potential

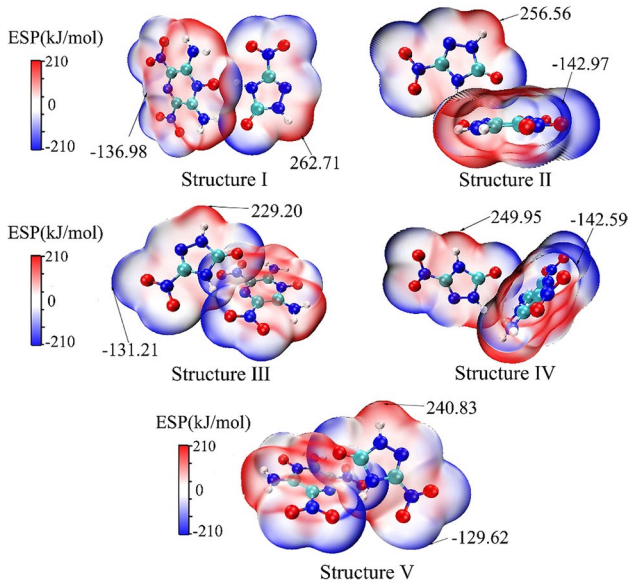

Fig. 7 Intermolecular van der Waals surface penetration graphs for electrostatic potential coloring of the five structures of NTO/LLM-105 complex

and LLM-105 molecules, which is consistent with the results of the above study.

Conclusions

Based on DFT, the intermolecular interaction between NTO and LLM-105 was studied using molten TNT as an implicit solvent for correction. The type, strength, and location of the interaction were discussed. The sensitivity changes of NTO/LLM-105 complexes were investigated. The main conclusions are as follows:

The intermolecular interactions between NTO and LLM-105 are mainly based on N–H…O type intermolecular hydrogen bonds and van der Waals, with H…O bond lengths ranging from 1.6826 to 2.0163 Å. The dominating intermolecular interactions between NTO and LLM-105 are H(6)…O(13) and H(2)…O(13). The interaction energies of the

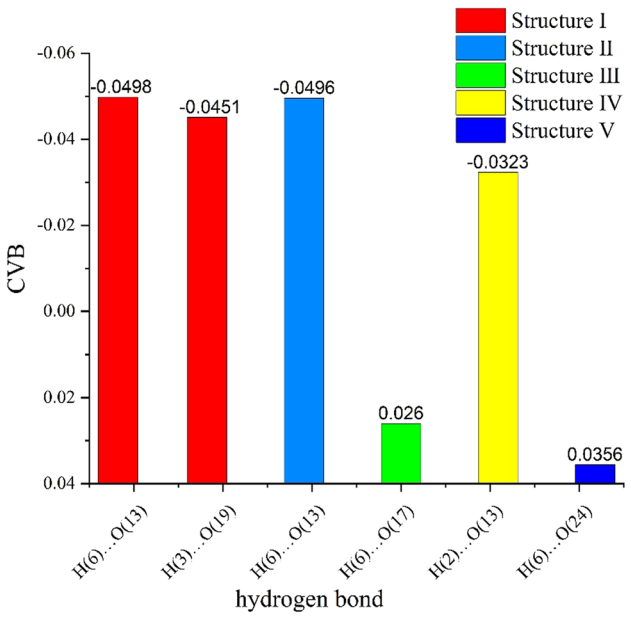

Fig. 8 CVB index diagram of hydrogen bonds in the five structures of NTO/LLM-105 complex

five NTO/LLM-105 structures are ranging from − 69.41 to − 53.64 kJ/mol. The stability of the five structures is ranked as follows: Structure I > Structure II > Structure IV > Structure III > Structure V. Moreover, Structure I is more stable than the NTO dimer or the LLM-105 dimer. The intermolecular hydrogen bond between NTO and LLM-105 contributes to the decrease in the acidity of NTO and the sensitivity of NTO/LLM-105 complexes. These desirable results indicated that the intermolecular interaction between NTO and LLM-105 provides an efficient guidance to explore more stable and safer melt cast explosives.

Acknowledgements We gratefully acknowledge the National Key Laboratory of Applied Physics and Chemistry for financial support.

Declarations

Conflict of interest The authors have no conflicts of interest to declare that are relevant to the content of this article.

References

Alipour M, Taravat F (2018) On the theoretical rationalization of intermolecular interactions: insights from DFT energy partitioning schemes. Theor Chem Acc 137:14. https://doi.org/10.1007/s00214-018-2349-2

Averkiev BB, Antipin MY, Yudin IL, Sheremetev AB (2002) X-ray structural study of three derivatives of dinitropyrazine. J Mol Struct 606:139–146. https://doi.org/10.1016/s0022-2860(01)00862-6

Bader RFW, Stephens ME (1975) Spatial localization of the electronic pair and number distributions in molecules. J Am Chem Soc 97:7391–7399. https://doi.org/10.1021/ja00859a001

Badgujar DM, Talawar MB (2017) Thermal and sensitivity study of dihydroxyl ammonium 5,5 ′-bistetrazole-1,1 ′-diolate (TKX-50)-based melt cast explosive formulations. Propellants Explos Pyrotech 42:883–888. https://doi.org/10.1002/prep.201600168

Badgujar DM, Talawar MB (2018) Thermokinetic decomposition and sensitivity studies of 4,4 ′-diamino-3,3 ′-azoxy furazan (DAAF)-based melt cast explosive formulations. J Energ Mater 36:316–324. https://doi.org/10.1080/07370652.2017.1421725

Badgujar DM, Talawar MB, Asthana SN, Mahulikar PP (2008) Advances in science and technology of modern energetic materials: an overview. J Hazard Mater 151(2–3):289–305. https://doi.org/10.1016/j.jhazmat.2007.10.039

Bolotina NB, Hardie MJ, Speer RL Jr, Pinkerton AA (2003) Energetic materials: variable-temperature crystal structure of b-NTO. J Appl Crystallogr 36:280–285. https://doi.org/10.1107/S002188980300092X

Cremer D, Kraka E (1984) Chemical Bonds without bonding electron density—does the difference electron-density analysis suffice for a description of the chemical bond? Angew Chem Int Ed 23:627–628. https://doi.org/10.1002/anie.198406271

Duarte LJ, Silva AF, Richter WE et al (2019) Infrared intensification and hydrogen bond stabilization: beyond point charges. J Phys Chem A 123:6482–6490. https://doi.org/10.1021/acs.jpca.9b03105

Firme CL (2021) Local potential energy density model (LPE): applications and limitations to quantify intra/intermolecular interactions. Comput Theor Chem 1197:7. https://doi.org/10.1016/j.comptc.2021.113143

Frisch MJ, Trucks GW, Schlegel HB (2009) Gaussian 09, revision A. 01, [CP]. Gaussian Inc, Wallingford CT

Gopalakrishnan S, Shankar R, Kolandaivel P (2018) DFT/TD-DFT study on the electronic and spectroscopic properties of hollow cubic and hollow spherical (ZnO)(m) quantum dots interacting with CO, NO2 and SO3 molecules. Appl Phys A-Mater Sci Process 124:13. https://doi.org/10.1007/s00339-018-1698-y

Grimme S (2011) Density functional theory with London dispersion corrections. Wiley Interdiscip Rev-Comput Mol Sci 1:211–228. https://doi.org/10.1002/wcms.30

Grimme S, Antony J, Ehrlich S et al (2010) A consistent and accurate ab initio parametrization of density functional dispersion correction (DFT-D) for the 94 elements H-Pu. J Chem Phys 132:19. https://doi.org/10.1063/1.3382344

HammamiIssaouiNasr FNS (2021) Investigation of hydrogen bonded structure of urea-water mixtures through Infra-red spectroscopy and non-covalent interaction (NCI) theoretical approach. Comput Theor Chem 1199:113218. https://doi.org/10.1016/j.comptc.2021.113218

Hang GY, Yu WL, Wang T et al (2018) Theoretical investigations on stabilities, sensitivity, energetic performance and mechanical properties of CL-20/NTO cocrystal explosives by molecular dynamics simulation. Theor Chem Acc 137:14. https://doi.org/10.1007/s00214-018-2297-x

Ji JC, Wang K, Zhu SM et al (2021) Structure, intermolecular interactions, and dynamic properties of NTO crystals with impurity defects: a computational study. CrystEngComm 23:2455–2468. https://doi.org/10.1039/d0ce01670e

Jun J, Jiayun L, Chen Yahong Wu, Zeyu QJ, Zhang S (2021) Detonation response mechanism of shocked LLM-105 using ReaxFF-lg and MSST. Mol Simul 47(8):678–687. https://doi.org/10.1080/08927022.2021.1902517

Kaur D, Khanna S (2011) Intermolecular hydrogen bonding interactions of furan, isoxazole and oxazole with water. Comput Theor Chem 963:71–75. https://doi.org/10.1016/j.comptc.2010.09.011

Klapötke TM (2021) Energetic materials encyclopedia. De Gruyter, Berlin. https://doi.org/10.1515/9783110442922

Lee K-Y, Chapman LB, Cobura MD (1987) 3-Nitro-1,2,4-triazol-5-one, a less sensitive explosive. J Energ Mater 5(1):27–33. https://doi.org/10.1080/07370658708012347

Li X, Wang BL, Lin QH (2016) Compatibility Study of 2,6-Diamino-3,5-dinitropyridine-1-oxide with Some Energetic Materials. Central Eur J Energ Mater 13:978–988. https://doi.org/10.22211/cejem/67312

Li X, Lin Qh, Peng Jh et al (2017) Compatibility study between 2,6-diamino-3,5-dinitropyrazine-1-oxide and some high explosives by thermal and nonthermal techniques. J Therm Anal Calorim 127:2225–2231. https://doi.org/10.1007/s10973-016-5809-8

Li JS, Chen JJ, Hwang CC et al (2019) Study on thermal characteristics of TNT based melt-cast explosives. Propellants Explos Pyrotech 44:1270–1281. https://doi.org/10.1002/prep.201900078

Li ZY, Luo B, Yu LZ et al (2021) Intermolecular B-N coordination and multi-interaction synergism induced selective glycoprotein adsorption by phenylboronic acid-functionalized magnetic composites under acidic and neutral conditions. J Mat Chem B 9:453–463. https://doi.org/10.1039/d0tb01901a

Liu Y, Rui-jun G, Shu-hai Z et al (2019) Solvent effect on the formation of NTO/TZTN cocrystal explosives. Comput Mater Sci 163:308–314. https://doi.org/10.1016/j.commatsci.2019.03.035

Lu T, Chen FW (2012) Multiwfn: A multifunctional wavefunction analyzer. J Comput Chem 33:580–592. https://doi.org/10.1002/jcc.22885

Lu T, Chen FW (2013) Bond Order Analysis Based on the Laplacian of Electron Density in Fuzzy Overlap Space. J Phys Chem A 117:3100–3108. https://doi.org/10.1021/jp4010345

Lu Tian, molclus program, Version1.9.9, http://www.keinsci.com/research/molclus.html

Mason HE, Guillen GJ, Gash AE (2019) Fast Magic-angle spinning solid-state H-1 NMR reveals structural relationships in the high explosive 2,6-diamino-3,5-dinitropyrazine-1-oxide (LLM-105). J Phys Chem C 123:21788–21795. https://doi.org/10.1021/acs.jpcc.9b06180

Mishra VS, Vadali SR, Bhagat AL et al (2017) Studies on NTO-, FOX-7-and DNAN-based melt cast formulations. Central Eur J Energ Mater 14:403–417. https://doi.org/10.22211/cejem/69397

Peterson PD, Lee KY et al (2007) The evolution of sensitivity in HMX-based explosives during the reversion from delta to beta phase. In: American Institute of Physics, AIP Conference Proceedings, vol 955, pp 987–990. https://doi.org/10.1063/1.2833297

Pina JJ, Gil DM, Perez H (2021) Revealing new non-covalent interactions in polymorphs and hydrates of Acyclovir: Hirshfeld surface analysis. NCI plots and energetic calculations. Comput Theor Chem 1197:113133. https://doi.org/10.1016/j.comptc.2020.113133

Powala D, Orzechowski A, Florczak B, Maranda A, Nowaczewski J (2006) Less sensitive explosives - 3-Nitro-1,2,4-triazol-5-one (NTO). Przem Chem 85(3):177–181

Ravi P, Badgujar DM, Gore GM et al (2011) Review on melt cast explosives. Propellants Explos Pyrotech 36:393–403. https://doi.org/10.1002/prep.201100047

Sarangapani R, Ramavat V, Reddy S et al (2015) Rheology studies of NTO-TNT based melt-cast dispersions and influence of particle-dispersant interactions. Powder Technol 273:118–124. https://doi.org/10.1016/j.powtec.2014.12.013

Smith MW, Cliff MD (1999) NTO-based explosive formulations: a technology review DSTO-TR-0796. Aeronautial Maritime Research Laboratory, Melbourne

Steiner T (2010) The hydrogen bond in the solid state. Angew Chem Int Ed 41:48–76. https://doi.org/10.1002/1521-3773(20020104)41:1%3c48::AID-ANIE48%3e3.0.CO;2-U

Trzcinski WA (2020) Study of shock initiation of an nto-based melt-cast insensitive composition. Propellants Explos Pyrotech 45:1472–1477. https://doi.org/10.1002/prep.202000050

Trzcinski WA, Lasota J, Chylek Z et al (2016) NTO-based melt-cast insensitive compositions. Central Eur J Energ Mater 13:592–611. https://doi.org/10.22211/cejem/65002

Vijayalakshmi R, Radhakrishnan S, Shitole P, Pawar SJ, Mishra VS, Garg RK, Talawar MB, Sikder AK (2015) Spherical 3-nitro-1,2,4-triazol-5-one (NTO) based melt-cast compositions: heralding a new era of shock insensitive energetic materials. RSC Adv 5:101647–101655. https://doi.org/10.1039/c5ra19010j

Waller MP, Yang J (2013) Revealing noncovalent interactions in quantum crystallography. Acta Crystallogr Sect A 69:S92–S92. https://doi.org/10.1107/s0108767313099194

Wang J, Shukla MK (2021) Density functional theory investigation on the degradation mechanisms of 3-nitro-1,2,4-triazol-5-one (NTO) in water. J Struct Chem 32:1357–1363. https://doi.org/10.1007/s11224-021-01795-x

Wang JK, Xiong Y, Li HZ et al (2018) Reversible hydrogen transfer as new sensitivity mechanism for energetic materials against external stimuli: a case of the insensitive 2,6-diamino-3,5-dinitropyrazine-1-oxide. J Phys Chem C 122:1109–1118. https://doi.org/10.1021/acs.jpcc.7b11393

Wu JT, Zhang JG, Li T et al (2015) A novel cocrystal explosive NTO/TZTN with good comprehensive properties. RSC Adv 5:28354–28359. https://doi.org/10.1039/c5ra01124h

Xiao H-M, Ju X-H, Xu L-N (2004) A density-functional theory investigation of 3-nitro-1,2,4-triazole-5-one dimers and crystal. J Chem Phys 121:12523–12531. https://doi.org/10.1063/1.1812258

Zhang C, Shu Y, Huang Y et al (2005) Investigation of correlation between impact sensitivities and nitro group charges in nitro compounds. J Phys Chem B 109:8978–8982. https://doi.org/10.1021/jp0512309

Zhang YP, Hou CH, Jia XL et al (2020) Compatibility study of 1,1-diamino-2,2-dinitroethene (FOX-7) with some energetic materials. J Chem 2020:7605140. https://doi.org/10.1155/2020/7605140

Zhu SF, Zhang SH, Gou RJ et al (2017) Theoretical investigation of the effects of the molar ratio and solvent on the formation of the pyrazole-nitroamine cocrystal explosive 3,4-dinitropyrazole (DNP)/2,4,6,8,10,12-hexanitrohexaazaisowurtzitane (CL-20). J Mol Model 23:14. https://doi.org/10.1007/s00894-017-3516-4